

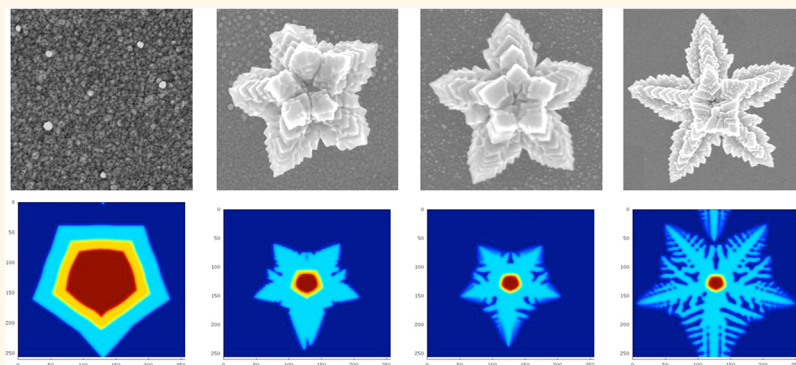
# pH-Dependent Evolution of Five-Star Gold Nanostructures: An Experimental and Computational Study

Zidong Wang,<sup>†</sup> Madurai Srinivasan Bharathi,<sup>‡</sup> Ramanarayanan Hariharaputran,<sup>‡</sup> Hang Xing, Longhua Tang,<sup>†,§</sup> Jinghong Li,<sup>§</sup> Yong-Wei Zhang,<sup>‡,\*</sup> and Yi Lu<sup>†,\*</sup>

<sup>†</sup>Departments of Materials Science and Engineering and Chemistry, University of Illinois at Urbana—Champaign, Urbana, Illinois 61801, United States,

<sup>‡</sup>Institute of High Performance Computing, A-STAR, Singapore, and <sup>§</sup>Department of Chemistry, Tsinghua University, Beijing 100084, China

## ABSTRACT



Dendritic structures, such as snowflakes, have been observed in nature in far-from-equilibrium growth conditions. Mimicking these structures at the nanometer scale can result in nanomaterials with interesting properties for applications, such as plasmonics and biosensors. However, reliable production and systematic fine-tuning morphologies of these nanostructures, with novel hierarchical or complex structures, along with theoretical understanding of these processes, are still major challenges in the field. Here, we report a new method of using pH to control  $\text{HAuCl}_4$  reduction by hydroxylamine for facile production of gold nanostructures with morphologies in various symmetries and hierarchies, both in solution and on solid surface. Of particular interest is the observation of five-star-like dendritic and hierarchical gold nanostructures under certain reaction conditions. Phase-field modeling was used to understand the growth and formation dynamics of the five-star and other gold complex nanostructures, and the results not only explained the experimental observations, but also predicted control of the nanostructural morphologies using both pH and hydroxylamine concentrations. In addition to revealing interesting growth dynamics in forming fascinating complex gold nanostructures, the present work provides a pH-directed morphology control method as a facile way to synthesize and fine-tune the morphology of hierarchical gold nanostructures.

**KEYWORDS:** five star · dendritic structure · shape evolution · gold nanostructures · phase-field modeling

**G**old nanostructures have been the subject of intensive research in recent years, due to their intriguing optical, electrical, and chemical properties.<sup>1,2</sup> These properties have allowed the gold nanostructures to be used in many biomedical science and engineering applications.<sup>3–7</sup> Because these properties are highly dependent on morphologies, such as shape and size, much effort has been devoted to control the morphologies of gold nanostructures. As a result, a large number of gold nanostructures of various morphologies including

nanospheres, nanorods, nanowires, nanoprisms, nanoplates and branched nanostructures have been synthesized.<sup>8–15</sup> To control the morphologies, different methods have been reported, including adjusting the reaction conditions (such as choice of the precursor materials, molecular ratio, or temperature) and employing selective adsorbates, such as surfactants, small molecules, or polymer capping agents, to control the nanocrystal growth.<sup>12,13</sup> Despite tremendous progress made in this area, it is still challenging to produce gold nanostructures

\* Address correspondence to  
yi-lu@illinois.edu;  
zhangyw@ihpc.a-star.edu.sg.

Received for review November 20, 2012  
and accepted February 26, 2013.

Published online February 26, 2013  
10.1021/nn305395p

© 2013 American Chemical Society

with hierarchical or complex structures, and it is even more difficult to systematically tune the morphology of these complex nanostructures.

Among the gold nanostructures with a high level of complexity, gold dendritic structures with hyperbranched architectures are particularly interesting. These structures exhibit superior physicochemical properties ideal for applications in plasmonics and biosensors due to their high surface area and the presence of nanoscale branches.<sup>16–25</sup> Dendritic structures have been prepared by ionic liquid templating,<sup>17</sup> solvothermal,<sup>21</sup> metal replacement,<sup>29</sup> or electrochemical method.<sup>23–25</sup> For example, an elegant approach reported by Kelley, Sargent and coworkers using electrochemistry was reported to change the morphology of the structure deposited on the electrode by adjusting electrochemical potentials or deposition time.<sup>25</sup> For industrial-scale applications, it is desirable to develop methods that are easier to scale up than the electrochemical method, such as using solution chemistry without the need of surfactants or templates. A few previous reports have shown that 5-fold symmetry could be observed as intermediates in nanocrystal growth.<sup>26,27</sup> Recently, Chen and co-workers have reported successful synthesis of 5-fold stellate polyhedral gold nanoparticles with {110} facets in aqueous solution *via* a seed-mediated growth method without adding surfactant.<sup>28</sup> Most of these studies reported the preparation of individual types of structures. Built on the success of these studies, it is important to demonstrate systematic tuning of such dendritic nanomaterials so that their physicochemical properties can be tailored for specific plasmonic and biosensing applications. Furthermore, our current understanding of the dendritic structural formation and its structural evolution has been elusive, and it is desirable to develop a computational method to study dendritic structures so that these structures, including new ones, can be predictably synthesized.

In nature, dendritic (or fractal) structures are observed ubiquitously in far-from-equilibrium growth conditions.<sup>29</sup> One interesting example is the formation of snowflakes from water vapors in the air, under supersaturation. To explain and analyze such fractal growth phenomena, diffusion-limited aggregation (DLA) and cluster–cluster aggregation (CCA) models have often been used.<sup>30–32</sup> The morphologies of a crystal are determined by the correlation between the driving force of crystallization and diffusion of atoms, ions, molecules, or heat. Theoretically, it is possible to tune the driving force of crystallization or the molecular diffusion rate to vary the crystal morphology. Dendritic growth of crystals results from the limitation of growth rate by the diffusion field and is controlled by the transport of material at moving interfaces (for example, the solid–liquid interface in the case of melt growth). Methods that track moving interfaces explicitly are highly impractical for complex morphologies such as

dendrites. An efficient method to address moving interfaces in complex morphologies is phase field modeling. Phase field models are based on the diffused interface, which is defined by an order parameter like density, composition, and orientation fields (phase field).<sup>27,33</sup> These order parameters change continuously from one phase to another with a finite interface width. Thus, the explicit tracking of the moving interface is not needed in this method. The phase-field method has been successful in explaining interface dynamics in many phenomena like melt growth,<sup>34–36</sup> grain growth, solid state phase transformation, crack propagation, and dislocation dynamics.<sup>37</sup>

Inspired by nature and motivated by their promising applications, herein we develop both a new experimental system and a new computational model for not only systematic tuning, but also a deeper understanding of gold nanostructures with snowflake-like or dendritic gold nanostructures both in solution and on solid surface. These morphologies can be fine-tuned systematically by simply adjusting the pH of the reaction system. At optimized conditions, gold crystals with controlled symmetries or snowflake-like gold nanostructures are formed, respectively, where some of these structures are brand new and not reported in literature. The formation of the snowflake-like gold nanostructures has also been explained by the phase-field method, thus, contributing to our fundamental understanding of this important class of complex dendritic structural formation.

## RESULTS AND DISCUSSION

Seed-mediated growth of gold nanoparticles is often carried out in aqueous solution by using HAuCl<sub>4</sub> gold precursor and hydroxylamine/ascorbic acid as the reductant. In work reported by Natan and co-workers, hydroxylamine was used to reduce HAuCl<sub>4</sub>, and they reported that HAuCl<sub>4</sub> reduction occurred only in the absence of gold nanospheres, and the reduction reaction could be catalyzed by a pre-existing gold surface.<sup>38</sup> In their experiments, the pH of the reaction system was acidic (pH 4). On the other hand, Peng and co-workers reported the shape of the resulting gold nanoparticle is pH-dependent in the seed-mediated approach, and gold nanoflowers were formed at higher pH by using gold nanospheres as seeds and hydroxylamine as reductant.<sup>39</sup> These studies suggested that pH could be used to tune gold nanostructures. We therefore first investigated the effect of pH on the reduction reaction in the absence of a gold surface. Because pure NH<sub>2</sub>OH is an unstable compound, easily decomposing to nitric oxide and hydrogen, we used its more stable form NH<sub>2</sub>OH·HCl in this study. Hydroxylamine solutions with different pH values (from 4.5 to 11) were prepared by titrating NH<sub>2</sub>OH·HCl with different aliquots of NaOH. HAuCl<sub>4</sub> was then introduced to each of the hydroxylamine solutions to initiate the reaction.

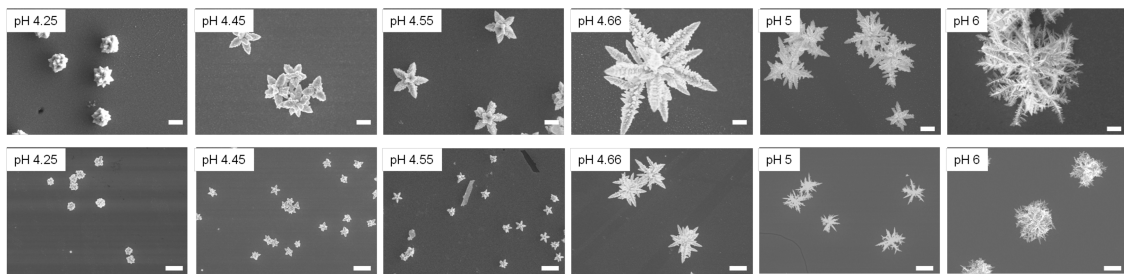


**Figure 1.** SEM images of the gold crystal structures grown at varying pHs (from left to right: pH 4.25, 4.45, 4.55, 4.66, 5, and 6). The images in the bottom row are larger scale images of the corresponding top row. The scale bars in the top row images indicate 500 nm. The scale bars in the bottom row images indicate 2  $\mu$ m.

Interestingly, the color of the resulting solutions at very high pH (pH 11) immediately changed from colorless to blue, while solutions with moderate pH (from 5.5 to 10.5) changed to gray in a few minutes. In contrast, those solutions with lower pH (<pH 5.5) remained colorless (see Figure S1).

Transmission electron microscopy (TEM) was then employed to investigate the morphology of the prepared gold crystals from each solution. For those solutions with pH lower than 5.5, very few metal structures were observed under TEM, and they were gold metal aggregations larger than 2  $\mu$ m in size (Figure S1b). When the pH was in the range of 5.5 to 10, dendritic gold structures were observed. When the pH reached 11, gold nanoflowers of size around 70 nm were observed. These results indicate that the reduction reactions, as well as the morphologies of the resulted gold nanocrystals, are pH-dependent. At higher pH, the reduction of HAuCl<sub>4</sub> by hydroxylamine is much faster than that of lower pH. This pH-dependence in reduction rate determined the formation of different-shaped gold crystals at different pH values.

Knowing that the reaction of HAuCl<sub>4</sub> with NH<sub>2</sub>OH is pH-dependent, we further extended our study on growing the gold structures in the presence of a gold surface. Cr layer (3 nm in thickness) and Au layer (30 nm in thickness) were deposited by using an E-beam evaporator on a round glass coverslip (5 mm in diameter). The freshly prepared gold surface was immersed in 300  $\mu$ L of NH<sub>2</sub>OH solution of varying pH, and then 3  $\mu$ L of 1% HAuCl<sub>4</sub> was added to initiate the reduction reaction. Hydroxylamine was kept in large excess over HAuCl<sub>4</sub> (molar ratio of NH<sub>2</sub>OH/HAuCl<sub>4</sub> > 60) and the reaction was carried out under room temperature for each reaction to eliminate the influence of other factors, such as temperature or ratio of the reagents, on the gold nanostructure morphology. Because the gold surface has been shown to catalyze the reduction of HAuCl<sub>4</sub> by hydroxylamine effectively under acidic condition,<sup>38</sup> a pH range of 4 to 6 was chosen to minimize the self-nucleation of gold atoms while the gold surface could still catalyze the reduction of HAuCl<sub>4</sub> by hydroxylamine. The reaction proceeded for 30 min before the surface was taken out for SEM characterization.

As shown in Figure 1, at pH 4.25, flower-like gold structures were observed under SEM. The gold crystals had a size of around 1  $\mu$ m. As the pH increased to 4.45, branched gold structures were observed. The number of tips ranged from 3 to 10. Interestingly, five-star gold structures, which are rarely observed in nature or under experimental conditions, were formed in low yields. At pH 4.55, however, the five-star gold structure was formed in higher yield (~30%), while most of the other formed gold structures had 6 to 10 extended tips. For the five-star gold structures, each tip was evenly extended out, with the angle between each adjacent tip at ~72°. When the pH in the reaction solution reached 4.66, gold structures with more than 10 tips were observed. With a further increase of pH to 5.00 or higher, dendritic gold structures with a number of branches formed. These results demonstrated that the pH value during gold structure growth has remarkable influence on the formed gold structure morphologies.

To investigate the dynamics of the growth process of the five-star gold structures, the above growth process was stopped by removing the gold surface from the reaction solution and rinsing immediately with water after the reaction, for different periods of time. The morphologies of the resulting structures were monitored under SEM. Figure 2 showed the time-dependent growth process of the five-star structures. After 1 min of reaction, only gold nanoparticles 20 nm in size were formed. After 5 min, the five-star structures were observed. As the reaction proceeded further along, the tips of the five-star extended longer. No further morphology change was observed when the reaction was extended for longer than 30 min. Energy-dispersive X-ray (EDX) spectral analysis (Figure S2) confirmed that the gold five-star nanostructure consisted of pure gold. In addition, we tried to grow this five-star gold nanostructure on some nongold surfaces, such as Si surface or Cr film surface. However, neither of these surfaces could produce gold five-star nanostructures (Figure S3), suggesting that the gold surface plays an important role in forming the five-star structures. This pH-directed morphology evolution of the gold structures suggests a new method to synthesize and tune the morphology of the hierarchical gold nanostructures.

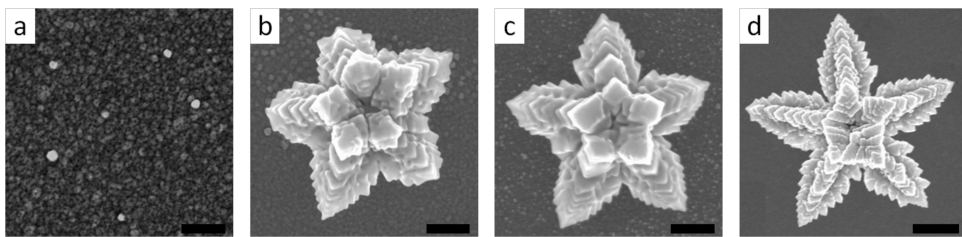


**Figure 2.** SEM images of the gold crystal structures formed at varying growth times: (a) 1, (b) 5, (c) 10, and (d) 30 min. The scale bars in the first three images from the left indicate 200 nm, and the scale bar in the right-most image indicates 500 nm.

A particularly interesting finding from this study is that the five-star gold structures formed only at certain pH. Theoretical understanding of its formation, however, is lacking.

To obtain an in-depth understanding of the growth process of the five-star gold structures, we have used a phase-field model based on the model proposed by Karma and Plapp<sup>40</sup> to simulate the growth of the gold dendrites. This model is written in terms of the surface height  $h$  (in units of interlayer width of the dendrites) and the concentration field  $u = \Omega(c - c_{eq})$ , where  $c$  is the concentration of gold adatoms,  $\Omega$  is the atomic area of the solid, and  $c_{eq}$  is the equilibrium concentration of the gold adatoms on the surface. The evolution equations for  $h$  and  $u$  are

$$\begin{aligned} \tau_h \frac{\partial h}{\partial t} &= -\frac{\delta G}{\delta h} \\ &= K^2 \nabla^2 h + \sin(\pi[h - h_0]) + \lambda u \{1 + \cos(\pi[h - h_0])\} \\ \frac{\partial u}{\partial t} &= D \nabla^2 u - \frac{u}{\tau_s} + F - \frac{1}{2} \frac{\partial h}{\partial t} \end{aligned}$$

Here,  $G$  is the free energy function depending on  $h$  and  $u$ ,  $h_0$  is the initial height of the surface,  $K$  is the gradient energy term,  $D$  is the isotropic diffusion coefficient, and  $F$  is the flux of the gold adatoms arriving at the surface.  $\tau_s$  is the mean lifetime of the gold adatom on the surface,  $\tau_h$  is the characteristic time of attachment of the adatoms to the surface, which is much smaller than  $\tau_s$ , and  $\lambda$  is a dimensionless coupling constant. The free energy,  $G$ , has minima at  $h - h_0 = 2n + 1$ , independent of  $u$ . The 5-fold symmetry is placed in the gradient term as  $K^2 = K^2 \{1 + \varepsilon \cos(n\theta)\}$ , where  $n = 5$  and  $K$  and  $\varepsilon$  are constants. The details of the simulation methods, including scaling and model parameters used, are described in the Simulation Method section. In this model, two system parameters, that is, the deposition flux  $F$  and diffusion coefficient  $D$ , are of particular importance in controlling the morphologies of the gold structures.

To correlate the experimental factors, such as pH and concentration of the reagents, with the parameters used in the simulation, such as the flux of Au adatoms and diffusion coefficient, we first looked into the influence of pH on hydroxylamine in the reaction

system. Hydroxylamine exists in the reaction solution in two chemical forms:  $\text{NH}_2\text{OH}$  or its protonated form  $\text{NH}_3\text{OH}^+$ .  $\text{NH}_2\text{OH}$  has a lower reduction potential and thus is oxidized easier by  $\text{HAuCl}_4$ .<sup>33</sup> Because the  $pK_a$  of  $\text{NH}_3\text{OH}^+/\text{NH}_2\text{OH}$  is 5.80–5.90, below the pH range used in our experiments (4.30–4.80), the majority of the hydroxylamine exists in the form of  $\text{NH}_3\text{OH}^+$ . With increasing pH, a significant portion of  $\text{NH}_3\text{OH}^+$  should be deprotonated and converted to  $\text{NH}_2\text{OH}$ , increasing the reaction rate, giving rise to a higher total flux of gold atoms. For example, based on the above  $pK_a$ , for the total concentration of  $\text{NH}_2\text{OH}$  at 20 mM, the effective concentration of  $\text{NH}_2\text{OH}$  increased from 0.61 mM at pH 4.30 to 1.06 mM at pH 4.55, then further to 1.82 mM at pH 4.80. With the increase of pH, however, more nuclei were generated so the effective flux per nucleus decreased. This hypothesis is supported by our experimental results on reacting  $\text{NH}_2\text{OH}$  of varying pH with  $\text{HAuCl}_4$  in solution and in the absence of external gold substrate (Figure S1). When the pH was lower than 6.00, the reaction solution remained clear, very few gold crystals could be found, and they were all larger than micrometer sizes. When the pH increased to 6.00–10.00, a gray color was produced after the first minute of reaction, and micrometer-sized dendritic gold structures were observed. As the pH reached 11.00 or higher, an instant change to blue color was observed after mixing  $\text{NH}_2\text{OH}$  with  $\text{HAuCl}_4$ , and only nanosized gold nanoparticles were observed, indicating the generation of a large number of nanosized nuclei. Thus, an increase in pH not only increases the flux of gold atoms, but also the number of nuclei formed. The flux of gold atoms,  $F$ , used in the phase-field model is the effective flux available per nucleus.

Next, we looked into the influence of pH on  $\text{HAuCl}_4$  in the reaction system.  $\text{HAuCl}_4$  exists in the forms of  $\text{AuCl}_4^-$  (>85%) and  $\text{AuCl}_4(\text{OH})^-$  (<15%) at pH 4.20–4.80.<sup>41</sup> Because the  $\text{AuCl}_4^-$  is more oxidative than  $\text{AuCl}_4(\text{OH})^-$  and is the dominating form with an effective concentration change less than 10% in the pH range of 4.20–4.80, the influence of pH on the  $\text{HAuCl}_4$  reactivity is much less than that on the  $\text{NH}_2\text{OH}$  reactivity. Therefore, the influence of pH on the reaction rate (and, thus, total flux rate) is mainly through  $\text{NH}_2\text{OH}$  rather than through  $\text{HAuCl}_4$  reactivity.

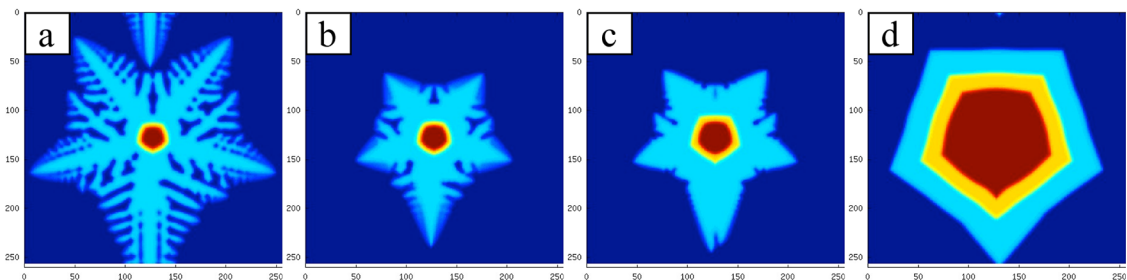


**Figure 3.** Effect of gold flux on the morphology: (a)  $F = 0.0002$ , (b)  $0.0006$ , (c)  $0.001$ , and (d)  $0.005$ .  $D = 6$  is used for all these simulations.

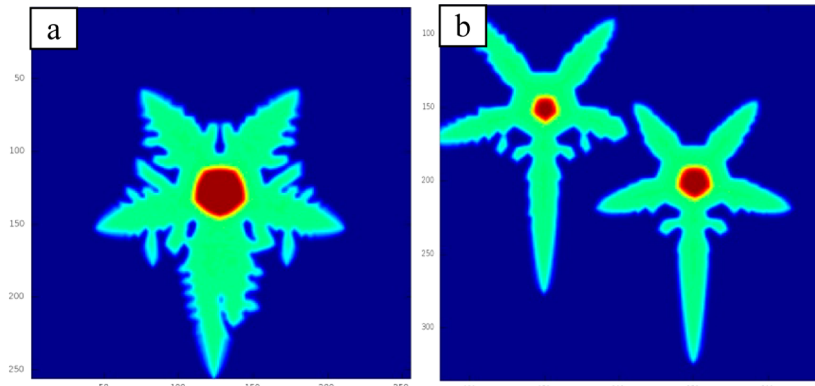


**Figure 4.** Simulation results showing the effect of multiple nucleations on the width of the dendritic arms. (a) Dendrite grown from one nucleus at  $F = 0.0004$  and (b) dendrites grown from two nuclei at  $F = 0.0005$ .  $D = 5$  for both the cases. The thinning of dendritic arms is clearly seen.

To provide a more quantitative understanding of the results obtained from the pH-dependent dendritic structural formation, we performed simulations in which the diffusion coefficient ( $D$ ) is used to determine the range of values for which the dendrites were observed. The simulations performed by varying  $D$  show that a decrease in diffusivity resulted in finer dendrites (Figure S4). The diffusion coefficient  $D$  of the gold adatoms in the phase-field model depends on both substrate material and reaction temperature. For a given substrate, there is an Arrhenius relation between temperature and  $D$ . For the same substrate and reaction temperature, it is reasonable to take  $D$  as a constant in the simulations. In Figure S4, we have shown the role of  $D$  on the dendrites, that is, dendritic width increases with increasing  $D$ . In our simulations,  $D$  is chosen to match the experimental dendritic patterns by varying the deposition flux. We find that  $D = 6$  gives the best match.

Figure 3 shows the simulation results for the dendritic patterns for  $D = 6$  and  $F$  ranging from 0.0002 to 0.005. The simulation predicts that, as the flux decreases, the dendrites become thinner. The experimental results shown in Figure 1 indicate thinner dendritic arms with increasing pH. Because increasing pH should theoretically result in a higher concentration of the reductant ( $\text{NH}_2\text{OH}$ ) *versus* its protonated form ( $\text{NH}_3\text{OH}^+$ ) and, thus, faster reduction and higher flux of

the gold atoms, the trend predicted by the computations shown, Figure 3, appears to contradict the experimental results in Figure 1. However, an increase in pH also increases the number of nuclei formed, thereby reducing the effective flux per nucleus. To understand the influence of the number of nuclei on the effective flux and, hence, the width of the dendrites, we performed simulations by starting with one and two nuclei, and the results are shown in Figure 4. Figure 4a shows the dendrite formed with one nucleus at  $F = 0.0004$  and Figure 4b shows the dendrites formed at  $F = 0.0005$  with two nuclei. We can clearly see that in the presence of more nuclei, the dendritic arms become thinner even when the flux is higher. The simulation therefore predicts that average flux *per nucleus* should decrease with the increase of pH or  $\text{NH}_2\text{OH}$  concentration and, thus, produce thinner and more dendritic structures. These simulation results correlate well with the experimental results that a higher pH produced more dendritic structures.

Furthermore, the presence of multiple nuclei can also explain the apparent loss of the 5-fold symmetry of the dendrites observed in Figure 1 for pH values greater than 4.60. Figure 5 shows the growth of dendrites when two nuclei are formed very close to each other. The 5-fold symmetry can be observed in the early stages. As they grow, however, these dendrites fuse together due to the lack of space to grow and the

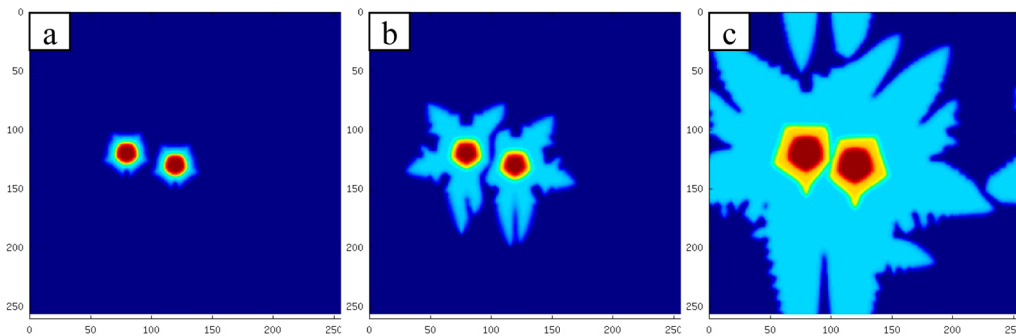


**Figure 5. Snapshots of the simulation results on the multiple nuclei and apparent loss of symmetry. Evolution of two closely spaced nuclei at  $F = 0.0006$  and  $D = 6$ ; (a)  $t = 200$ , (b) 1500, and (c) 5000, in units of  $\tau_h$ .**

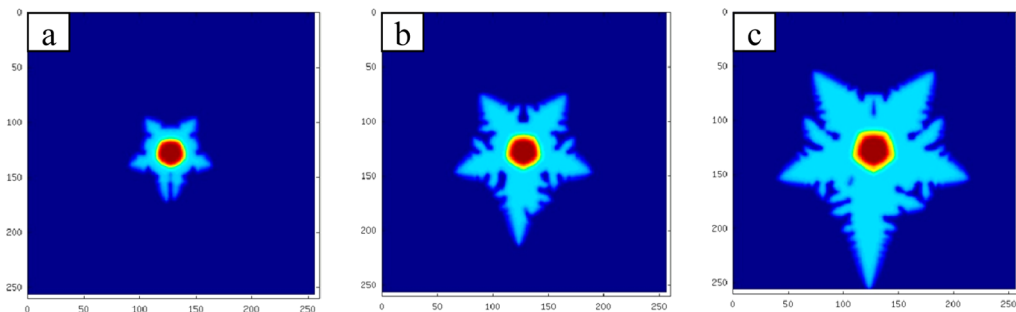


**Figure 6. Snapshots of the simulation results on the time-dependent growth of gold structures for  $F = 0.0006$  and  $D = 5$ : (a)  $t = 1000$ , (b) 2000, and (c) 3000, in units of  $\tau_h$ .**

symmetry appears to be lost. Therefore, these results suggest that the morphology of the dendrites is influenced not only by the flux of the gold atoms but also the number of nuclei formed.

Based on the above simulation results that show the influence of pH on the reaction rate is mainly through adjusting the effective  $\text{NH}_2\text{OH}$  concentration, we hypothesize that both the pH and the  $\text{NH}_2\text{OH}$  concentration can be used to tune the reaction rate, the nucleation density, and thus, dendritic structural morphologies. At a pH where effective  $\text{NH}_2\text{OH}$  concentration is lower, five-star structures can still be formed if we increase the total  $\text{NH}_2\text{OH}/\text{NH}_3\text{OH}^+$  concentration added to the reaction mixture. On the other hand, at high pH where effective  $\text{NH}_2\text{OH}$  concentration is higher, less total  $\text{NH}_2\text{OH}/\text{NH}_3\text{OH}^+$  concentration is required to form the five-star structures. At intermediate pH, only a moderate concentration of total  $\text{NH}_2\text{OH}/\text{NH}_3\text{OH}^+$  is required. To test this simulation-based hypothesis, we grew gold nanostructure under the following three different conditions: high concentration (50 mM)  $\text{NH}_2\text{OH}$  at low pH (pH 4.30), low concentration (10 mM)  $\text{NH}_2\text{OH}$  at high pH (pH 4.80), and intermediate concentration (20 mM  $\text{NH}_2\text{OH}$ ) at intermediate pH (pH 4.55). As shown in Figure S5, all three tested conditions produced similar five-star structures, even though the gold structures produced at higher pH were larger than those at lower pH. Therefore, we can conclude that both the pH and  $\text{NH}_2\text{OH}$  concentration work in combination to achieve the same morphological effects.

After using computations to explain and then predict thermodynamic effects of pH on the five-star structure, we turned our attention to use simulations to explain the time-dependent five-star structure growth using time-dependent flux change during the reaction. For an optimized condition in the gold structure growth, the concentration of  $\text{HAuCl}_4$  (210  $\mu\text{M}$ ) is much lower than the  $\text{NH}_2\text{OH}$  concentration (10, 20, or 50 mM). In the presence of gold substrate, all the  $\text{HAuCl}_4$  should be reduced to gold metals, while the concentration of  $\text{NH}_2\text{OH}$  does not change significantly. As the reaction proceeds, the concentration of  $\text{HAuCl}_4$  decreases gradually to zero. Therefore, for a given reaction, the flux of gold adatoms decreases with gold crystal growth time. The simulation results (Figure 6) correlate with experimental results (Figure 2) very well.

Finally, the evolution of the dendrites in Figure 2 clearly shows the presence of multiple layers of dendritic growth. The morphologies shown in these figures suggest that the multiple layers grew due to subsequent nucleation on the higher layers. To simulate this growth of multiple layers, we started with a circular seed with height of 1 unit. We then initiated further nucleation on this layer at a rate of 0.1 per unit area on the dendrite. Once the area of the first layer of the dendrite grew more than 10 square units, we initiated a second circular seed with a height of 3 units at the center of the dendrite and then allowed the dendrites to evolve. The results of these simulations for  $D = 5$  and  $F = 0.0003$  are shown in Figure S6 at times

$t = 1500$  (Figure S6a) and  $t = 3000$  (Figure S6b). The evolution of the dendrites shown in this figure supports our assumption that subsequent nucleation on the dendritic layers resulted in multilayer growth.

## CONCLUSION

We have demonstrated a new method of using pH to grow hierarchical gold nanostructures with controlled morphology both in solution and on a surface. We have identified that pH played an important role in controlling the reduction rate, as well as the gold nanocrystal morphology. By growing the gold structures on the solid surface, we have achieved further control of the gold crystal morphology, mimicking the growth process of snowflakes. Both pH and reagent concentration were used to fine-tune the gold structures with controlled symmetry, and five-star like gold structures were prepared under certain reaction conditions. The phase-field model was used to simulate and predict

the growth of five-star and other complex gold structures, and the simulation results correlated well with the experimental results. In general, a phase-field model can explain and predict the growth kinetics and morphological evolution in a qualitative manner since many system parameters in the model are difficult to determine. The good correlation between our experimental and simulation results rests on the fact that we have established a good correspondence between the experimental factors, such pH and concentration of the reagents, and the modeling parameters, such as the flux of Au adatoms and diffusion coefficient. The pH-directed morphology control method demonstrated here provides a facile way to synthesize and fine-tune the morphology of the hierarchical gold nanostructures systematically, allowing these gold nanostructures to be used in applications such as electronics, catalysis, sensing, and imaging.

## MATERIALS AND METHODS

**pH-Dependent Shape Evolution in Solution.** Hydroxylamine (20 mM) solution was first adjusted to different pH values (from 4 to 12) using concentrated sodium hydroxide. Then, 100  $\mu$ L of each solution was transferred into centrifuge tubes individually, followed by the addition of 1  $\mu$ L of 1%  $\text{HAuCl}_4$  solution to initiate the reaction. After 30 min of reaction, each solution was dropped on a TEM grid and imaged using a transmission electron microscope.

**Gold Crystal Growth on a Flat Gold Surface.** E-beam evaporator was used to deposit a 3 nm Cr adhesive layer and 30 nm gold layer on a round glass coverslip (5 mm in diameter) at a deposition rate of 1  $\text{\AA}$  per second. The cleanliness of the gold surface is critical to the successful growth of the gold structures, and the gold structure growth should be carried out with a freshly made gold surface, preferably in a cleanroom. The gold-coated glass coverslip was put in 300  $\mu$ L 20 mM  $\text{NH}_2\text{OH}$  solution of various pH, and then 3  $\mu$ L 1%  $\text{HAuCl}_4$  solution was added to the  $\text{NH}_2\text{OH}$  solution to initiate the reduction. The reactions were made for at least 30 min at room temperature before sample preparation for imaging. For kinetic studies, the reactions were stopped by taking out the surface and rinsing with pure water at 1, 5, 10, and 30 min time points. After nitrogen blowing to dry the surfaces, these surfaces were imaged under scanning electron microscopy (SEM) at 15 kV.

**Simulation Method.** The phase-field equations are solved by discrete Fourier transform method.<sup>40</sup> We use periodic boundary conditions in the  $x$  and  $y$  directions and solve for  $h(x,y,t)$ . In our simulations we use the phase-field units for length and time measurements,<sup>14</sup> that is,  $K^2 = 1$  and  $\tau_h = 1$ . The equations are discretized in both space and time, and we used  $\Delta x = \Delta y = 1$  and  $\Delta t = 0.01$  in our simulations. All the results shown here are for a system size of  $256 \times 256$  units, unless otherwise mentioned. The parameters used are  $\tau_s = 1000000.0$ ,  $\lambda = 10$ , and  $\varepsilon = 0.04$ . We take the equilibrium concentration  $c_{\text{eq}} = u(x,y,0) = 0.5$ . Starting with a cylindrical nucleus of height 5 units and radius 10 units on a flat surface of height  $-1$ , the simulations are carried out at different values of flux  $F$ .

**Conflict of Interest:** The authors declare no competing financial interest.

**Acknowledgment.** We wish to thank Professor Y. Huang from Northwestern University for stimulated discussions and J. Wu for her help with EDX analysis. This work has been supported by the U.S. National Science Foundation (DMI-0328162)

and the Agency for Science, Technology and Research (A\*STAR), Singapore.

**Supporting Information Available:** Experimental details, simulation methods, and figures are given. This material is available free of charge via the Internet at <http://pubs.acs.org>.

## REFERENCES AND NOTES

- Daniel, M. C.; Astruc, D. Gold Nanoparticles: Assembly, Supramolecular Chemistry, Quantum-Size-Related Properties, and Applications toward Biology, Catalysis, and Nanotechnology. *Chem. Rev.* **2004**, *104*, 293–346.
- Rosi, N. L.; Mirkin, C. A. Nanostructures in Biodiagnostics. *Chem. Rev.* **2005**, *105*, 1547–1562.
- Jin, R.; Cao, Y.; Mirkin, C. A.; Kelly, K. L.; Schatz, G. C.; Zheng, J. Photoinduced Conversion of Silver Nanospheres to Nanoprisms. *Science* **2001**, *294*, 1901–1903.
- Sonnichsen, C.; Reinhard, B. M.; Liphardt, J.; Alivisatos, A. P. A Molecular Ruler Based on Plasmon Coupling of Single Gold and Silver Nanoparticles. *Nat. Biotechnol.* **2005**, *23*, 741–745.
- Huang, X.; El-Sayed, I. H.; Qian, W.; El-Sayed, M. A. Cancer Cell Imaging and Photothermal Therapy in the Near-Infrared Region by Using Gold Nanorods. *J. Am. Chem. Soc.* **2006**, *128*, 2115–2120.
- Lu, Y.; Liu, J. Smart Nanomaterials Inspired by Biology: Dynamic Assembly of Error-Free Nanomaterials in Response to Multiple Chemical and Biological Stimuli. *Acc. Chem. Res.* **2007**, *40*, 315–323.
- Wang, Z.; Lu, Y. Functional DNA Directed Assembly of Nanomaterials for Biosensing. *J. Mater. Chem.* **2009**, *19*, 1788–1798.
- Sun, Y.; Xia, Y. Shape-Controlled Synthesis of Gold and Silver Nanoparticles. *Science* **2002**, *298*, 2176–2179.
- Busbee, B. D.; Obare, S. O.; Murphy, C. J. An Improved Synthesis of High-Aspect-Ratio Gold Nanorods. *Adv. Mater.* **2003**, *15*, 414–416.
- Wiley, B.; Sun, Y.; Chen, J.; Cang, H.; Li, Z.-Y.; Li, X.; Xia, Y. Shape-Controlled Synthesis of Silver and Gold Nanostructures. *MRS Bull.* **2005**, *30*, 356–361.
- Millstone, J. E.; Métraux, G. S.; Mirkin, C. A. Controlling the Edge Length of Gold Nanoprisms via a Seed-Mediated Approach. *Adv. Funct. Mater.* **2006**, *16*, 1209–1214.
- Tao, A. R.; Habas, S.; Yang, P. Shape Control of Colloidal Metal Nanocrystals. *Small* **2008**, *4*, 310–325.

13. Xia, Y.; Xiong, Y.; Lim, B.; Skrabalak, S. E. Shape-Controlled Synthesis of Metal Nanocrystals: Simple Chemistry Meets Complex Physics? *Angew. Chem., Int. Ed.* **2009**, *48*, 60–103.
14. Wang, Z.; Zhang, J.; Ekman, J. M.; Kenis, P. J. A.; Lu, Y. DNA-Mediated Control of Metal Nanoparticle Shape: One-Pot Synthesis and Cellular Uptake of Highly Stable and Functional Gold Nanoflowers. *Nano Lett.* **2010**, *10*, 1886–1891.
15. Wang, Z.; Tang, L.; Tan, L. H.; Li, J.; Lu, Y. Discovery of the DNA “Genetic Code” for Abiological Gold Nanoparticle Morphologies. *Angew. Chem., Int. Ed.* **2012**, *51*, 9078–9082.
16. Lu, G.; Li, C.; Shi, G. Synthesis and Characterization of 3D Dendritic Gold Nanostructures and Their Use as Substrates for Surface-Enhanced Raman Scattering. *Chem. Mater.* **2007**, *19*, 3433–3440.
17. Qin, Y.; Song, Y.; Sun, N.; Zhao, N.; Li, M.; Qi, L. Ionic Liquid-Assisted Growth of Single-Crystalline Dendritic Gold Nanostructures with a Three-Fold Symmetry. *Chem. Mater.* **2008**, *20*, 3965–3972.
18. Liebau, M.; Janssen, H. M.; Inoue, K.; Shinkai, S.; Huskens, J.; Sijbesma, R. P.; Meijer, E. W.; Reinhoudt, D. N. Preparation of Dendritic Multisulfides and Their Assembly on Air/Water Interfaces and Gold Surfaces. *Langmuir* **2002**, *18*, 674–682.
19. Fang, J.; Ma, X.; Cai, H.; Song, X.; Ding, B. Nanoparticle-Aggregated 3D Monocrystalline Gold Dendritic Nanostructures. *Nanotechnology* **2006**, *17*, 5841–5845.
20. Huang, K.; Zhang, Y.; Han, D.; Shen, Y.; Wang, Z.; Yuan, J.; Zhang, Q.; Niu, L. One-Step Synthesis of 3D Dendritic Gold/Polypyrrole Nanocomposites via a Self-Assembly Method. *Nanotechnology* **2006**, *17*, 283–288.
21. Wu, K.; Yu, R.; Li, X.; Wei, X. Magnetic and Catalytic Properties of Ni<sub>33</sub>Co<sub>67</sub> Alloy With Snowflake-Like Morphology Prepared by a Facile Solvothermal Method. *Micro Nano Lett.* **2012**, *7*, 685–688.
22. Sun, X.; Hagner, M. Novel Preparation of Snowflake-like Dendritic Nanostructures of Ag or Au at Room Temperature via a Wet-Chemical Route. *Langmuir* **2007**, *23*, 9147–9150.
23. Jing, Q.; Fu, W.; Li, W.; Yang, H.; Li, M.; Ma, J.; Zhou, X.; Sun, M.; Zhao, H.; Zhang, Y.; et al. Synthesis of Snowflake-Like Multi-Layered ZnO with Controllable Pore Sizes and its Photocatalytic Property. *Appl. Surf. Sci.* **2012**, *258*, 3604–3610.
24. Liu, J.; Fu, Y. Y.; Guo, A.; Wang, C.; Huang, R.; Zhang, X. Growth of Gold Fractal Nanostructures by Electrochemical Deposition in Organic Electrolytes: Morphologies and Their Transitions. *J. Phys. Chem. C* **2008**, *112*, 4242–4247.
25. Soleymani, L.; Fang, Z.; Sargent, E. H.; Kelley, S. O. Programming the Detection Limits of Biosensors Through Controlled Nanostructuring. *Nat. Nanotechnol.* **2009**, *4*, 844–848.
26. Jadzinsky, P. D.; Calero, G.; Ackerson, C. J.; Bushnell, D. A.; Kornberg, R. D. Structure of a Thiol Monolayer-Protected Gold Nanoparticle at 1.1 Å Resolution. *Science* **2007**, *318*, 430–433.
27. Van der Waals, J. D. *Verhandel. Konink. Akad. Weten.* **1893**, *1*, 56.
28. Jiang, L.; Tang, Y.; Liow, C.; Wu, J.; Sun, Y.; Jiang, Y.; Dong, Z.; Li, S.; David, V. P.; Chen, X. Synthesis of Fivefold Stellate Polyhedral Gold Nanoparticles with {110}-Facets via a Seed-Mediated Growth Method. *Small* **2012**, *10*.1002/smll.201202561.
29. Nanev, C. N. Polyhedral Instability - Skeletal and Dendritic Growth. *Prog. Cryst. Growth Charact. Mater.* **1997**, *35*, 1–26.
30. Witten, T. A.; Sander, L. M. Diffusion-Limited Aggregation. *Phys. Rev. B* **1983**, *27*, 5686–5697.
31. Meakin, P. Formation of Fractal Clusters and Networks By Irreversible Diffusion-Limited Aggregation. *Phys. Rev. Lett.* **1983**, *51*, 1119–1122.
32. Witten, T. A.; Sander, L. M. Diffusion-Limited Aggregation: a Kinetic Critical Phenomenon. *Phys. Rev. Lett.* **1981**, *47*, 1400–1403.
33. Cahn, J. W.; Hilliard, J. E. Free Energy of a Nonuniform System. 1. Interfacial Free Energy. *J. Chem. Phys.* **1958**, *28*, 258–267.
34. Karma, A.; Rappel, W. J. Phase-Field Method for Computationally Efficient Modeling of Solidification with Arbitrary Interface Kinetics. *Phys. Rev. E* **1996**, *53*, R3017–R3020.
35. Collins, J. B.; Levine, H. Diffuse Interface Model of Diffusion-limited Crystal Growth. *Phys. Rev. B* **1985**, *31*, 6119–6122.
36. Langer, J. S. G.; Mazenko, G. *Directions in Condensed Matter Physics*; World Scientific: Philadelphia, 1986; p164.
37. Chen, L. Q. Phase-Field Models for Microstructure Evolution. *Annu. Rev. Mater. Res.* **2002**, *32*, 113–140.
38. Brown, K. R.; Natan, M. J. Hydroxylamine Seeding of Colloidal Au Nanoparticles in Solution and on Surfaces. *Langmuir* **1998**, *14*, 726–728.
39. Zhao, L.; Ji, X.; Sun, X.; Li, J.; Yang, W.; Peng, X. Formation and Stability of Gold Nanoflowers by the Seeding Approach: The Effect of Intraparticle Ripening. *J. Phys. Chem. C* **2009**, *113*, 16645–16651.
40. Karma, A.; Plapp, M. Spiral Surface Growth Without Desorption. *Phys. Rev. Lett.* **1998**, *81*, 4444–4447.
41. Peck, J. A.; Tait, C. D.; Swanson, B. I.; Brown, G. E. Speciation of Aqueous Gold(III) Chlorides From Ultraviolet/Visible Absorption and Raman Spectroscopies. *Geochim. Cosmochim. Acta* **1991**, *55*, 671–676.